Effect of Packing on Void Morphology in Resin Transfer Molded E-Glass/Epoxy Composites

Youssef K. Hamidi, Levent Aktas, M. Cengiz Altan
School of Aerospace and Mechanical Engineering, University of Oklahoma, Norman, Oklahoma 73019

Effects of applying a packing pressure on void content, void morphology, and void spatial distribution were investigated for resin transfer molding (RTM) E-glass/epoxy composites. Packing pressures of zero and 570 kPa were respectively applied to center-gated composites containing 17.5% randomly oriented, E-glass fiber preform. Radial samples of these disk-shaped composites were utilized to evaluate voidage via microscopic image analysis. Two adjacent surfaces were cut from each molded disk in order to evaluate void presence from both through-the-thickness and planar views. The packed composite was found to contain almost 92% less void content than the unpacked composite. While void fractions of 2.2 and 2.6% were measured, respectively, from the through-the-thickness and planar surfaces of the unpacked composite, only 0.2% void content was observed in the packed composite from both surfaces. Digital images obtained from through-the-thickness surface showed that average void size dropped from 59.3 μm in the unpacked composite to 31.7 μm in the packed composite. A similar reduction in average void size from 66.7 to 41.1 μm was observed from the planar surfaces. Circular voids were found to experience higher removal rates at 99%, followed by cylindrical and elliptical voids at 83 and 81%, respectively; while irregular voids show slightly lower void removal rates at 67%. Void proximity to fiber bundles was also observed to affect void reduction as voids located inside fiber tows experience lower void reduction rates. Along the radial direction of the molded disks, removal of voids with different proximities to fibers seems to depend on their arrangement at the end of the filling stage. These findings are believed to ascertain packing as an effective void removal method for RTM and similar liquid composite molding processes. **POLYM. COMPOS., 26:614–627, 2005. © 2005 Society of Plastics Engineers**

INTRODUCTION

Liquid composite molding (LCM) processes such as resin transfer molding (RTM) have been established in the automotive and aerospace industries as versatile technologies for manufacturing medium to large composite parts with complex geometries [1–3]. RTM consists of injecting a reactive liquid resin into a closed mold cavity preloaded with layers of fibrous preform. After cure reaction is complete, the solidified composite part is removed from the mold. The relatively high occurrence of process-induced defects such as poor wet-out and voids during mold filling often limits the increased use of LCM and RTM in the composites industry. The presence of voids is known to shorten the service life of composites by reducing their thermomechanical performance [4–12] and adversely affecting their response to environmental effects [13, 14]. Despite the importance of voids, methods of void removal and their effectiveness are not fully established for LCM and RTM processes [3–6, 8, 12, 15–26].

Voids in RTM are primarily formed by the impregnation mechanisms of the unsaturated fibrous media during mold filling. Although the preform impregnation at macroscale is commonly described by a Darcy flow [27, 28], two different flows develop at different scales: 1) a viscous flow between fiber tows; and 2) a capillary flow inside each fiber bundle, driven by capillary forces. When these two flows are advancing at disparate front velocities, voids form by so-called mechanical entrapment [18–26]. At higher fill rates, the viscous flow leads the impregnation, and voids are mostly formed inside fiber tows via fingering or lead-lag phenomena, resulting in microscopic intra-tow voids. In contrast, at slower injection velocities the capillary flow leads the impregnation, and macroscopic inter-tow voids are formed between fiber tows. A minimum void occurrence can be obtained when both flows are advancing at comparable front velocities. Numerous researchers used flow visualization to monitor air entrapment during filling and documented this microscale flow behavior in detail [18–22].

In order to analyze the equilibrium between these two flows, Mahale et al. [19] used the capillary number, defined as the ratio of viscous to capillary forces. The authors reported that if the filling is performed at a capillary number of 2.5×10^{-3}, void formation will be minimal. Patel et al. [21], and Rohatgi et al. [22] generalized the nondimensional capillary number by introducing the liquid–fiber contact angle. Several researchers explained their experimental void

Correspondence to: M. Cengiz Altan; e-mail: altan@ou.edu
DOI 10.1002/pc.20132
Published online in Wiley InterScience (www.interscience.wiley.com).

formation data with the modified capillary number [24, 29, 31], thus establishing the capillary number analysis as an available method for predicting void formation in RTM and LCM composites. Other theoretical and numerical models have been offered for predicting void occurrence in liquid injection processes [32–37]. Yet these models have limited range of application, as they are generally developed for simplified preform architectures.

Although acceptable void levels can be achieved at optimum capillary numbers [8, 17–22], attaining such values often requires a range of injection rates slower than those used in the industry [29]. Slow injection rates increase mold filling time, and hence reduce RTM applicability to large-scale production. Thus, there is a need for effective void reduction or removal methods suitable for RTM processes involving fast injection rates.

Numerous techniques have been used to reduce void presence in composites manufactured by RTM and its variants [3, 8, 18–22, 25–29, 39–42]. Lunsdstrom et al. [25, 26], among others, utilized vacuum assistance to lower void content. The mold cavity is vacuumed before injection to lower the internal air pressure, hence facilitating void dissolution into the resin, and also enhancing void mobility during molding. Increasing the pressure difference between the inlet and outlet of the mold cavity from 0.17 to 0.50 MPa resulted in a decrease in void content from 6.5 to 3.8%. Yet low void contents are only reached when costly, very high vacuum levels are used [25].

Degassing the injected resin is also used to reduce voidage in molded composites, since high initial bubble content results in elevated void presence [3, 4, 12, 39]. However, resin degassing does not address entrapment by the fluid front, the primary cause of void formation for these processes. Another commonly used method for void removal is bleeding, which consists of continuing resin discharge after impregnation is completed to purge formed voids [18, 25, 40]. Bleeding might be useful when the formed voids are transportable, i.e., when voids are dominantly inter-tow voids. However, inter-tow voids are formed mostly at slow injection rates not seen in most industrial molding applications [19–22]. In addition, intra-tow voids formed in RTM processes with faster impregnation rates are found very difficult to purge by bleeding [22].

Another void removal method is compression, which consists of compressing mold walls after resin injection is complete [41]. Squeezing mold walls is anticipated to expel voids and help fabricate void-free composites. The method drives out voids only to the end of the cavity [11], and yet requires expensive tooling that might make the molded parts much more expensive. Articulated tooling, a variant of compressing mold walls, was recently proposed by Choi and Dharan [42]. This technique calls for a segmented articulated mold wall, utilized to sequentially impregnate dry preform areas in a stepwise, sequential manner. A 5-fold reduction in mold fill time and reduced void generation were observed [42]. Nonetheless, like compression, articulated tooling requires higher initial investment, and possibly yields undesirable surface marks and defects.

Packing is performed by a sudden increase in pressure after the molding cavity is filled. This method has also been used to reduce void occurrence in RTM composites [8, 18, 25, 29]. Forcing more resin into a previously filled mold cavity would shrink the existing voids or even dissolve them into the resin matrix. In an earlier study by Olivero et al. [8], void content was found to decrease exponentially with increasing applied packing pressure up to 700 kPa for resin transfer molded glass/epoxy composites at 21% fiber content [8]. In a different study performed at higher injection rates [29], applying a packing pressure as low as 300 kPa resulted in a drop of more than 70% in void content. Packing facilitates void removal for RTM and similar processes without additional tooling or investment. Hence, packing can be a cost-effective void removal technique that might improve most LCM processes. Concerns with packing reside in the possible spatial concentration of voidage or creation of large irregular voids with sharp corners that are prone to early failure cracks [11, 13]. To address this issue, a thorough investigation of the effects of packing on void morphology is needed. To the best of the authors' knowledge, no such study is available in the literature.

There are primarily two types of void studies relevant to molded polymeric composites: 1) postcure studies, conducted on actual molded composites; and 2) void formation studies, conducted by monitoring flow front progression during the impregnation process. Investigation of voids in molded composites can be conducted by a multitude of methods. However, void morphology is usually assessed by microscopic image analysis. Although microscopic image analysis is reported as one of the best methods to measure void contents [8, 43, 44], the obtained void morphology is only two-dimensional, as void data are generally collected from a polished through-the-thickness surface of the composite [7–9, 24, 28–30, 43, 44]. On the other hand, most studies on the mechanisms of void formation are conducted by monitoring flow front progression from the planar view [1, 2, 19, 21–23, 33, 35]. In addition, the filling process is usually carried out by using model fluids such as glycerin, ethylene glycol, and silicone and diphenyl-octyl-phthalate (DOP) oils. Although this technique provides valuable insight on void formation mechanisms such as fingering and lead-lag, it only captures 2D features of voids. Furthermore, model fluids do not cure and continue microscale impregnation due to capillary forces even after complete mold filling. Thus, the obtained void morphology might be affected by phenomena that are not present in curing resin mixtures.

In the current study, effects of applying a 570 kPa packing pressure on void content, void morphology, and void spatial distribution are investigated for resin transfer molded E-glass/epoxy composites. Voidage was assessed by microscopic image analysis of planar and through-the-thickness surfaces of the studied composites. Difference in void content and void areal density between the molded

composites was evaluated. In addition, changes in void morphology (i.e., size and shape) due to packing were investigated. Furthermore, radial variations in void content were examined, as well as changes in reduction rates based on void proximity to fibers.

EXPERIMENTAL SETUP

Molding Procedure

The composite disks used in this study were fabricated by a custom-made experimental molding setup composed of a hydraulic press, two reservoirs for resin and curing agent, a static mixer, and a disk-shaped mold cavity. Operating the molding press forces the EPON 815C resin and EPICURE 3282 (Shell Chemicals, Houston, TX) curing agent out of the reservoirs into the mold cavity at a constant flow rate. Thorough mixing of these fluids is ensured by the 32 alternating helical segments of a static mixer, yielding a gel time of ~20 min. Preforms placed in the mold cavity prior to filling are composed of four layers of the randomly oriented, chopped-strand, E-glass fiber mats with a planar density of 0.4356 kg/m^2 ± 0.0449 kg/m^2 (Fiberglast part #250). The details of the molding procedure and experimental setup are described in detail elsewhere [28–31]. The first resin transfer molded disk is manufactured without applying any packing pressure and is referred to as the unpacked composite. The second disk, referred to as the packed composite, is manufactured by applying a 570 kPa postfill pressure. The packing process forces additional resin into the mold cavity and induces a 2% increase in average composite thickness from 3.88 mm in the unpacked composite to 3.96 mm in the packed one. Both composites have around 17.5% fiber content by volume.

Sample Preparation for Microscopic Image Analysis

The planar isotropy of the fibrous preform and the mold axisymmetry simplify the impregnation into a purely radial flow. Hence, molded composite disks are examined along their radii. In order to prepare specimens for microscopic image analysis, two adjacent radial strips are cut from each disk. One of the strips is utilized for voidage assessment using its planar surface, and the other is used for void analysis based on its through-the-thickness surface. Figure 1 illustrates the spatial arrangement of these two strips obtained from both packed and unpacked composites. The first 2-mm-wide samples (Fig. 1b) are selected to investigate voidage from a planar surface, while the second ones (Fig. 1c) are utilized for void analysis from the through-the-thickness surface. All samples are 75-mm long, while the unpacked and packed composites have an average thickness of 3.88 and 3.96 mm, respectively. Radial variation of voidage is assessed by dividing each 75-mm-long sample into five 15-mm-long regions along the radial direction as shown in Fig. 1b,c. Composite strips are embedded separately into a quick cure acrylic resin (Allied High Tech Products, Rancho Dominguez, CA; part 170). The samples containing the planar composite surfaces are machined on a vertical mill to remove a thin layer and eliminate near-surface nonuniformities. For polishing, a series of polishing pastes are applied (Clover Compound) with grit sizes ranging from 180 (i.e., 80 μm average particle diameter) to 1200 (15 μm) in six successive steps. To remove paste residues after each step, 40 min of subsequent cleaning periods are performed in an ultrasonic bath at 50 kHz. After all polishing steps are completed, a 0.67-mm-thick layer is removed from the top of both planar composite samples. At the end of polishing and cleaning the samples become ready for microscopic image analysis.

Void Characterization

Microscopic image analysis is considered among the most precise methods for measuring void contents [8, 29, 43, 44]. In addition, this technique provides detailed information on other vital parameters such as void location, shape, and size that cannot be assessed by other methods. Often, microscopic image analysis is used by averaging randomly selected images [43, 44]. In the current investigation, however, the entire studied composite cross-sections were scanned in order to accurately estimate void content, morphology, and their spatial variations. Voidage features are obtained from images acquired at 200× magnification using a PC-based CCD camera mounted on a MEIJI optical microscope. At this particular magnification every frame displays approximately a 0.71 × 0.53 mm area. The selected magnification of 200× enables the assessment of voids as small as the radius of a single fiber of 7 μm. Consequently, all identifiable voids throughout the entire composite samples were included in the analysis of void content and morphology. Each captured frame was processed using the image analysis software UTHSCSA Image Tool, which allows the measurement of voids' area, A, and maximum length, L_{max}.

RESULTS AND DISCUSSION

Inlet Mold Filling Pressure

Temporal variation of molding pressure is monitored with a flush diaphragm pressure transducer (Sensotec BP357BR Model S, 0.1% accuracy), attached between the static mixer and the mold inlet. Due to the circular mold geometry and the preform planar isotropy, the resin front has a circular shape and advances radially through the preform. Molding takes place at a constant flow rate, thus, closer to the injection gate the resin front moves at higher velocities. The constant flow rate forces the inlet pressure to increase in order to impregnate a larger preform area as the flow front moves radially outward. Inlet pressure data recorded during filling of both packed and unpacked composite disks are shown in Fig. 2.

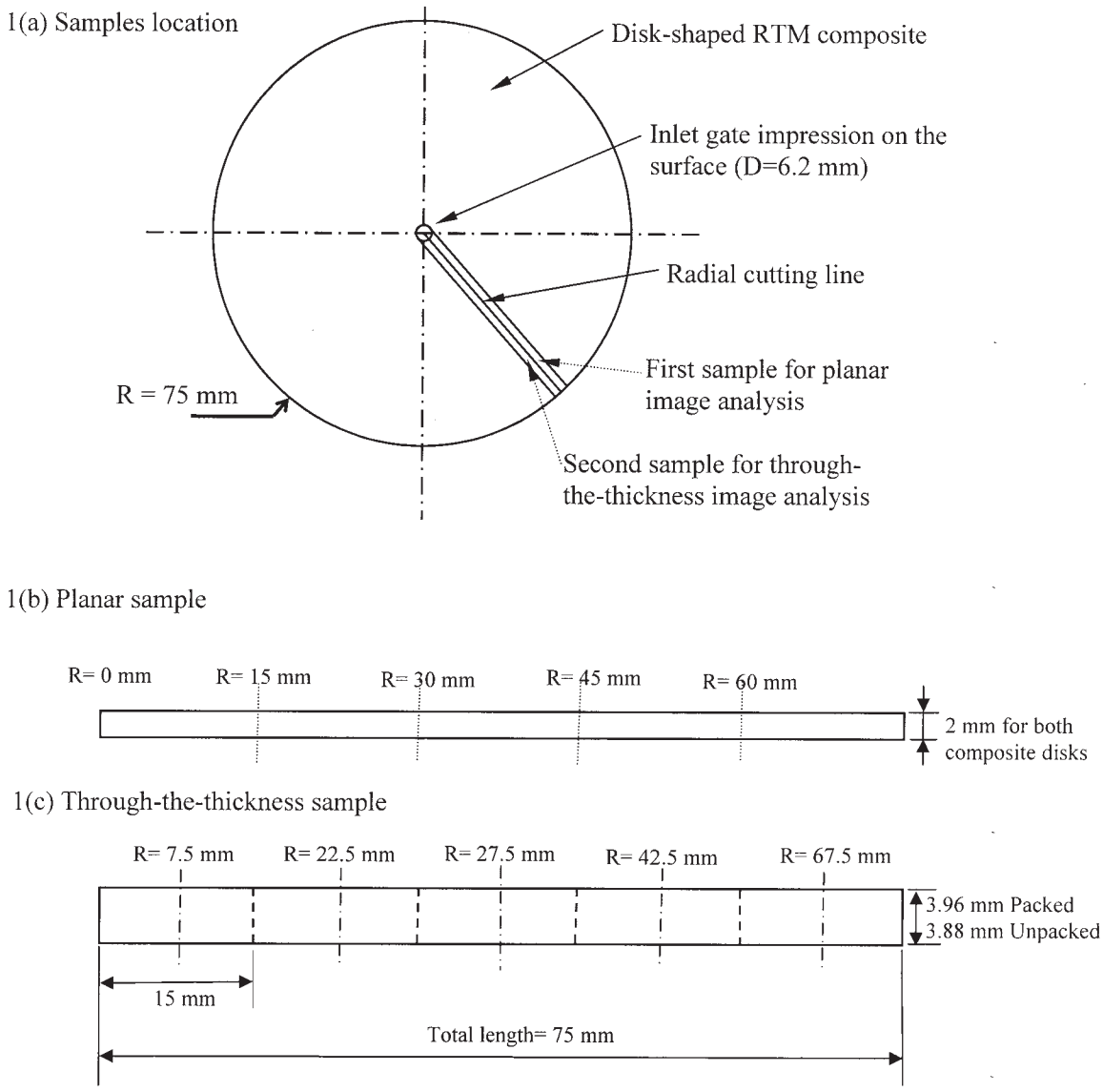

FIG. 1. Spatial arrangement of investigated samples for packed and unpacked composite disks: (a) sample locations within the composite disk, (b) planar sample partitions of five 15-mm-long radial regions, (c) through-the-thickness sample partitions of five 15-mm-long radial regions.

During the first 9 sec of mold filling the inlet pressures increase at similar rates for unpacked and packed composites. Thereafter, pressure readings show minor discrepancies due to slight variations in the constricted channel spacing between mold walls and spacer plates. Once the resin reaches the exit vents the molding press is turned off, stopping resin injection. As seen in Fig. 2, when the injection is stopped a monotonic decrease in pressure is recorded. This decrease is consistent with the natural predisposition of the system to reach a balance between inlet and outlet pressures. In the case of unpacked composite, exit vents are left open, hence the pressure continues decaying asymptotically to atmospheric pressure for 100 sec. The same behavior is observed for the packed composite during the 4 sec between the time injection is stopped and all vents are securely closed, thus sealing the mold. Thereafter, the pres-

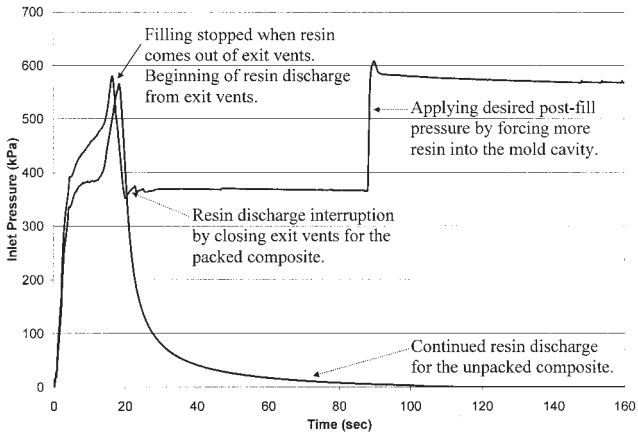

FIG. 2. Inlet pressure profiles during molding of the unpacked and packed composite disks.

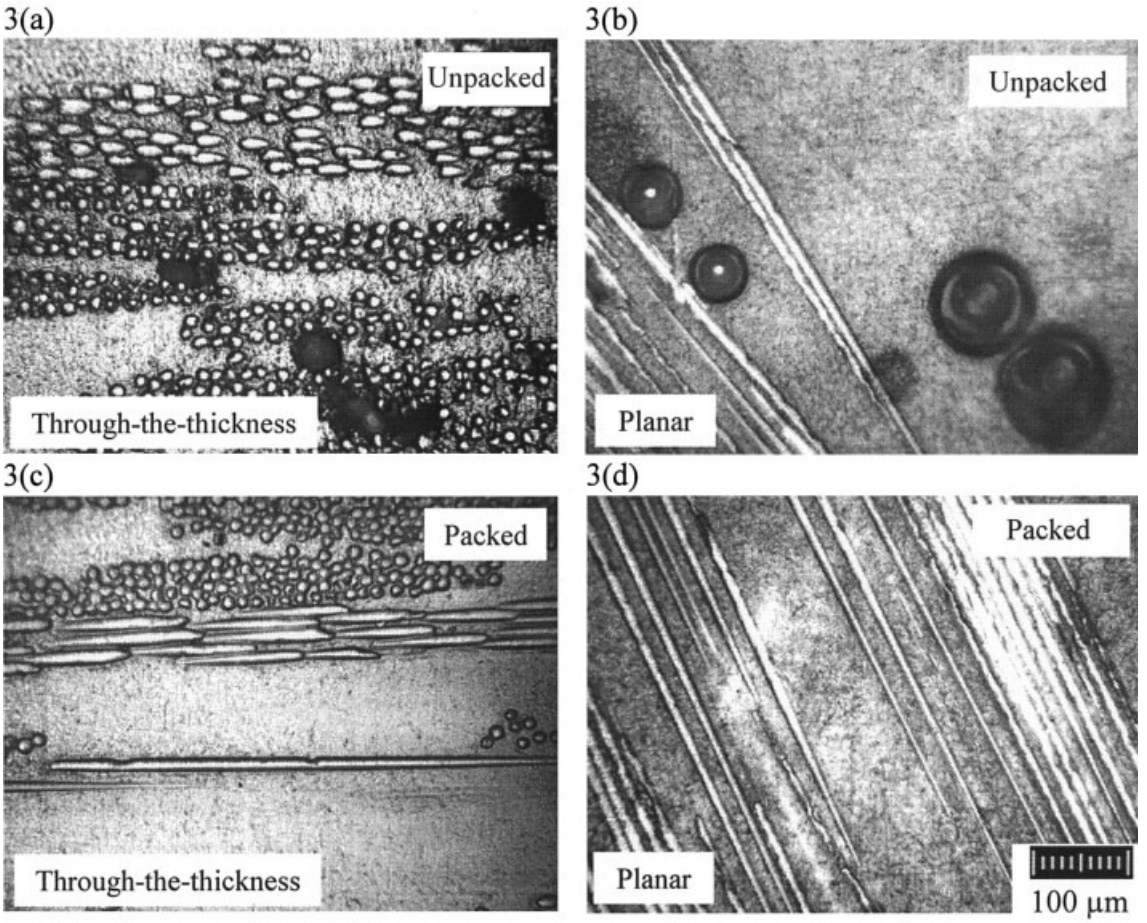

FIG. 3. Representative images of voids in different composite locations obtained at 200× magnification from through-the-thickness (left column) and planar (right column) views of the unpacked (top row) and packed (bottom row) composite disks.

sure is monitored for 60 sec. The pressure levels off to a plateau of 370 kPa, and remains constant until packing. Applying the desired postfill pressure of 570 kPa is achieved by forcing additional resin into the mold cavity, which requires operating the molding press for an additional 3 seconds. Inlet pressure is again monitored for 60 sec to ensure that no leaking occurs. Several minutes after the postfill pressure is applied the injection port is securely clamped and the composite is allowed to cure at the desired packing pressure. The slight pressure difference observed during filling of packed and unpacked composites is not likely to affect void morphology at the end of the filling stage. However, the application of the 570 kPa packing pressure is expected to reduce void content and induce major changes in void morphology and spatial distribution.

Assessment of Void Removal

Void contents from both unpacked and packed composites are assessed via microscopic image analysis. Representative images obtained at 200× magnification from both planar and through-the-thickness views of the unpacked and packed composites are depicted in Fig. 3. The continuous gray background in Fig. 3 represents the epoxy matrix, while the white circular and elliptical objects are glass fibers oriented perpendicularly and at an angle, respectively, to the cross-section. The single white parallel stripe in Fig. 3c and all others in Fig. 3d represent glass fibers parallel to the investigated cross-section. Figure 3a–d also depicts the basic difference in fiber orientation and clustering observed on planar and through-the-thickness surfaces of an RTM composite. Fibers are seen as more homogeneously distributed through the composite thickness, while the planar view offers large matrix-rich regions and other zones with high fiber concentration. Hence, different morphological features of voids are expected to become prominent when observed on these two orthogonal planes.

Void contents and void areal densities of the unpacked and packed composites are shown in Fig. 4. Results obtained from both planar and through-the-thickness views of each composite disk are presented. Analysis of through-the-thickness surfaces reveals that applying a 570 kPa postfill pressure resulted in a 91.2% reduction in the void content dropping from 2.2 to 0.2%. When the void contents obtained from planar surfaces are compared a similar 91.8%

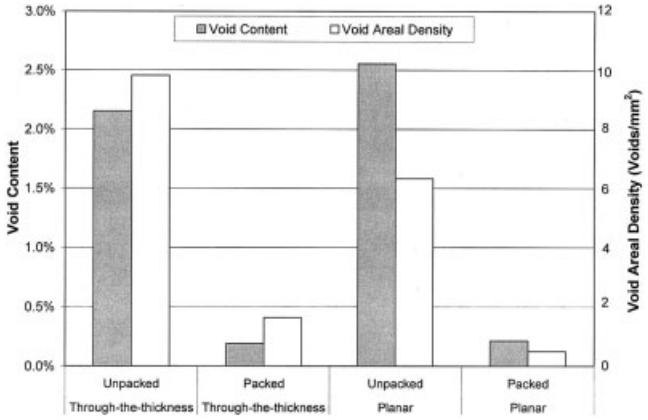

FIG. 4. Through-the-thickness and planar void contents and void areal densities for the unpacked and packed composite parts.

decrease from 2.6 to 0.2% is observed. This reduction in void content is accompanied with more than an 83 and 97% reduction in void areal density when assessed from the through-the-thickness and planar views, respectively. This large diminution in voidage is attributed primarily to void shrinkage and dissolution due to pressure differential between the resin and air trapped inside the voids. Packing is hereby ascertained as an efficient void reduction technique that removes the majority of voids formed during impregnation in liquid injection processes. Additional investigation is needed in order to understand relevant removal mechanisms, as well as the effects of packing on void morphology.

Effect of Packing on Void Location

As illustrated in Fig. 3, voids are seen at three different locations within the molded composites. The first location is defined as areas rich in matrix away from fibers. Voids encountered in this location are completely surrounded by the epoxy matrix and are referred to as matrix voids. The second location is defined as areas rich in preform, where the area is primarily composed of reinforcing fibers. Voids in this region are intra-tow voids situated within fiber bundles and are referred to as preform voids. Finally, the third location is defined as the transitional areas between the two other locations herein defined. Voids in this location are referred to as transition voids and are always positioned next to fiber bundles but not within the fiber preform. Based on the locations defined above, all voids present in Fig. 3a are preform voids. The two voids appearing in the left half of Fig. 3b are considered transition voids. Finally, the remaining two voids seen in the right of Fig. 3b are categorized as matrix void. Voids from these three different locations in the four composite samples are identified and their respective contributions to the total void content determined.

Figure 5 shows a reduction in void content in different locations of the packed composite, including results from both planar and through-the-thickness views. When assessed from the planar view, the 91.8% reduction in overall composite void content presented in Fig. 4 is not equally distributed among voids from the three locations defined above. Matrix and preform voids seem to experience higher reduction rates of 96.6 and 93.3%, respectively; while only a 79.4% reduction is observed for transition voids. The percentage reduction in void content observed through-the-thickness is also different among the three void locations. Both matrix and transition voids are reduced at a slightly higher rate of 93.3 and 94.7%, respectively. In contrast, preform voids are reduced only by 84.7%.

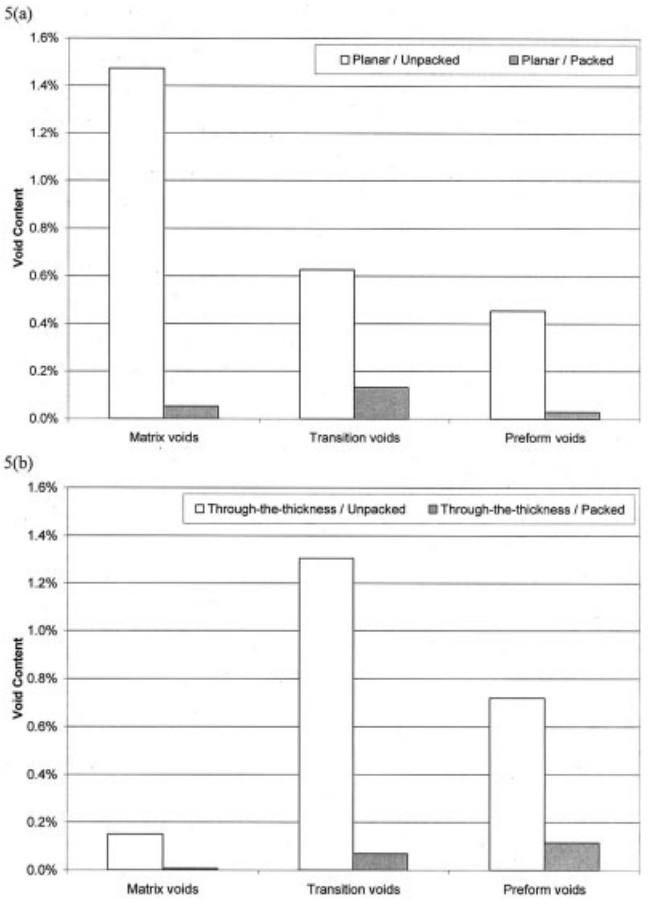

FIG. 5. Contributions from voids in different locations within the composite disks to the void contents of unpacked and packed parts viewed from: (a) the planar view, and (b) the through-the-thickness view.

This difference in perceived reduction of voids from different locations is believed to originate from the difference in void location distribution between planar and through-the-thickness views of the unpacked composite. Due to the planar architecture of the reinforcing preform, many voids that are classified as matrix voids in the planar view might be in contact with fibers at composite layers above or below the observed plane, belonging in fact to transition voids, as shown in Fig. 5b. Therefore, distribution of void location based on through-the-thickness surface is believed to be more representative of the actual distribution. Hence, the actual locations of voids throughout the composite would be better characterized from the through-the-

thickness view. In addition, location of voids based on the through-the-thickness view reveals that voids are concentrated either inside or right next to fiber bundles, as predicted for the local capillary number values [30, 31]. On the contrary, location distribution of voids based on the planar view depicts voids as mainly inter-tow, matrix voids.

In terms of void areal density, the void content reduction rates seen in Fig. 5b translate to 84.9 and 86.6% removal rates for matrix and transition voids, respectively, while preform voids are removed slightly less, at 78.8%. This is expected since intra-tow preform voids, once formed, are known to be more difficult to eliminate than inter-tow voids [10, 18, 22, 29], as they are trapped in the constricted narrow spacing within fiber bundles. As a result, preform voids see more than a 70% jump in their relative contribution to the total void content due to packing, increasing from 33.5 to 57.9% of the total voids.

Effect of Packing on Void Size

To classify void sizes, an equivalent diameter, D_{eq}, is defined for each void as:

$$D_{eq} = \sqrt{\frac{4A}{\pi}}, \tag{1}$$

where A is the void area measured via image analysis software UTHSCSA Image Tool. Similar methods are commonly used to characterize grain size in a multitude of materials such as metals [45, 46], ceramics [47–50], and polycrystalline materials [51, 52].

Figure 6a, obtained from images of the planar surface, illustrates void size distributions based on D_{eq} for both unpacked and packed composites. As a result of applying the 570 kPa packing pressure, the size distribution of voids is significantly changed. A large shift in void size distribution is observed as average void size is reduced from 66.7 μm in the unpacked composite to 41.1 μm in the packed composite. The highest void occurrence frequency changed from 16.2% for voids with D_{eq} between 60 and 70 μm in the unpacked composite to 25.3% for voids with D_{eq} between 20 and 30 μm in the packed composite.

Similarly, void size distributions obtained from the through-the-thickness view for both unpacked and packed composites are represented in Fig. 6b. Compared to Fig. 6a, a larger shift in void size distribution is observed as average void size decreases from 59.3 to 31.7 μm. The highest void occurrence frequency changed from 17.0% for voids with D_{eq} between 40 and 50 μm in the unpacked composite to 30.6% for voids with D_{eq} less then 20 μm in the packed composite.

In order to focus on other aspects of void size distributions, three different size ranges are defined. Large voids are defined as those with an equivalent diameter greater than 100 μm, i.e., $D_{eq} > 100$ μm, while voids with an equivalent diameter lower than 50 μm are regarded as small voids. Intermediate equivalent diameter values, i.e., 50 μm $< D_{eq} \leq 100$ μm, correspond to medium-size voids. Data obtained from voids in different composite locations are reprocessed using these three void sizes to quantify the effects of packing on size distribution of voids encountered in each composite location. Size distributions of matrix, transition, and preform voids obtained from planar surface data of unpacked and packed composites are presented in Fig. 7a. Likewise, size distributions of matrix, transition, and preform voids obtained from through-the-thickness surface data of unpacked and packed composites are presented in Fig. 7b.

When assessed from the planar view, i.e., Fig. 7a, small voids encountered within the matrix increase from 21.0% in the unpacked composite to more than 58% in the packed composite, while medium voids see their contribution reduced from 69.6 to 25.0%. This 77.4% increase in relative percentage of small voids found within the matrix along with the 64.0% decrease in medium matrix voids is a direct result of void shrinkage. From through-the-thickness view, i.e., Fig. 7b, an even accentuated trend is observed as small matrix voids augment from a relative frequency of 33.3% in the unpacked composite to almost 97% in the packed one. Medium matrix voids contribution is dramatically reduced due to packing from 61.3 to merely 3.0%, while large matrix voids completely disappeared in the packed composite.

As shown in Fig. 7a, size distribution of preform voids show a similar trend due to packing. The relative contribution of small preform voids, obtained from the planar view, depict a considerable increase from 40.4 to 68.0%. An opposite trend is observed for both medium and large voids, whose relative percentages drop from 49.2 and 10.4% to 28.0 and 4.0%, respectively. A decrease in average size of preform voids is also observed from the through-the-thickness view in Fig. 7b. Small intra-tow voids exhibit a 30.0% increase from 66.0% in the unpacked composite to 86.0% in the packed composite. Medium and large voids contributions, however, are decreased from 28.7 and 5.4% to 10.0 and 4.1%, respectively. The relatively smaller reduction in size of preform voids as compared to that of matrix voids seen from both views can be expected since intra-tow voids are physically trapped inside fiber tows, and hence might not be fully subjected to the higher packing pressure.

Difference between planar size distributions of transition voids of unpacked and packed composites, depicted in Fig. 7a, is the most interesting. Unexpectedly, large void frequency is observed to increase from merely 9.7% to 36.0%. At the same time, medium voids occurrence is reduced from 58.1% to 28.0% and the small void contribution is modestly increased from 32.3 to 36.0%. A more reasonable decrease in contribution of transition voids is observed from through-the-thickness view, i.e., Fig. 7b. Small transition voids augmented from 24.3% in the unpacked composite to 88.4% after packing. The medium transition voids contribution is considerably reduced from 67.1 to 11.6%, while no large transition voids are encountered in the through-the-thickness surface of the packed composite. These findings sug-

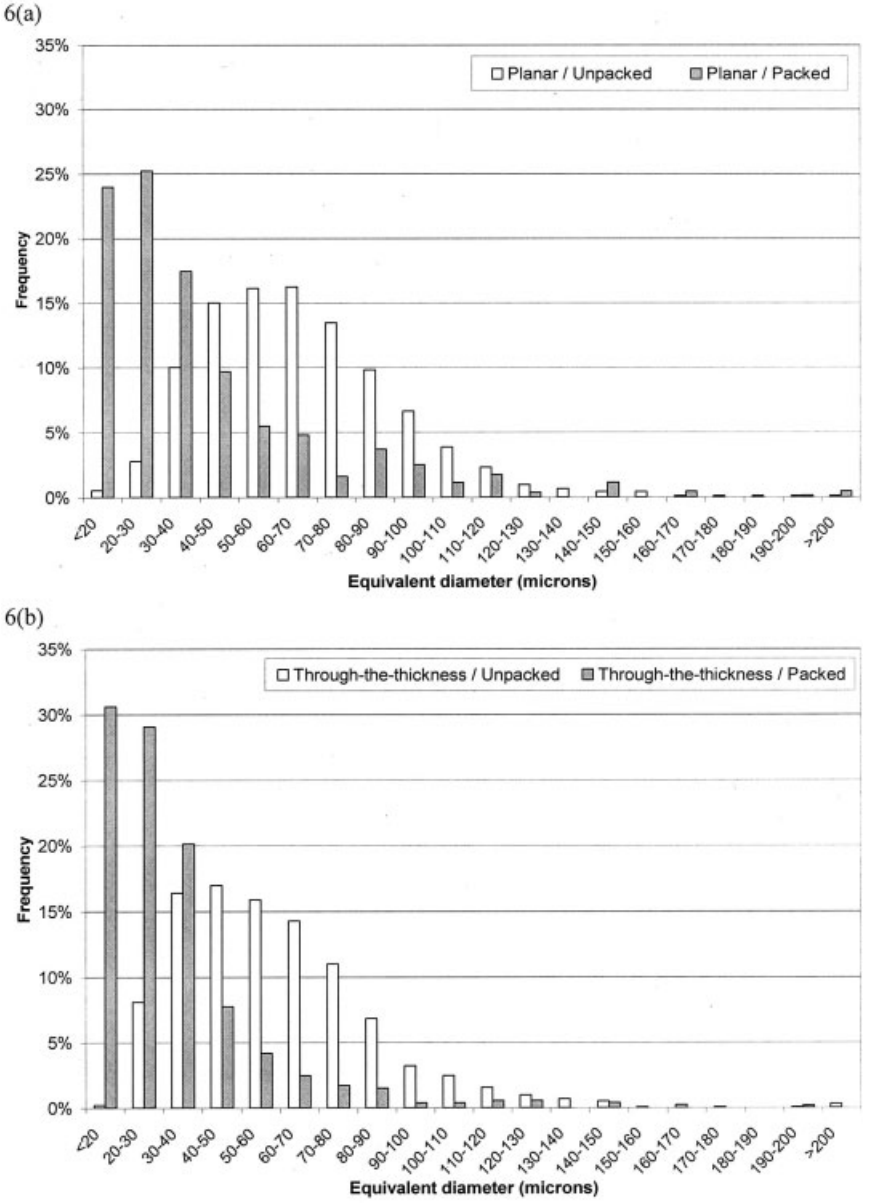

FIG. 6. Void size distributions for the unpacked and packed composite disks from: (a) the planar view; and (b) the through-the-thickness view.

gest that large voids trapped right next to the fiber bundles are more difficult to remove by packing than matrix voids, and perhaps that some transition voids consolidate together between planar preform layers into larger elongated voids. Although no explanation is found for this phenomenon solely based on Fig. 7a,b, a more careful look into the captured microscopic images of the packed composite shows that indeed most large transition voids—seen from the planar view—are deformed into irregular shapes, while no large transition voids are observed from through-the-thickness view. Nevertheless, these voids only sum up to less then 0.003% void content, which is by all means an insignificant occurrence that is not likely to alter the composite's mechanical performance. In summary, the investigation of void size distributions in both packed and unpacked composites shows that voids encountered in different composite locations do not respond equally to packing, but more importantly, that no critical adverse effect is introduced by applying a packing pressure.

Effect of Packing on Void Shape

Due to variations in void sizes and locations, a variety of void shapes are encountered in RTM composites [4, 20–25]. Howe et al. [4] reported the existence of two major void shapes for RTM woven carbon/epoxy composites at 59% fiber content. The first comprises spherical to elliptical voids with a diameter of 100–200 μm, and the second represents larger voids confined to the preform. These irregularly shaped voids have a height of 150–400 μm and a

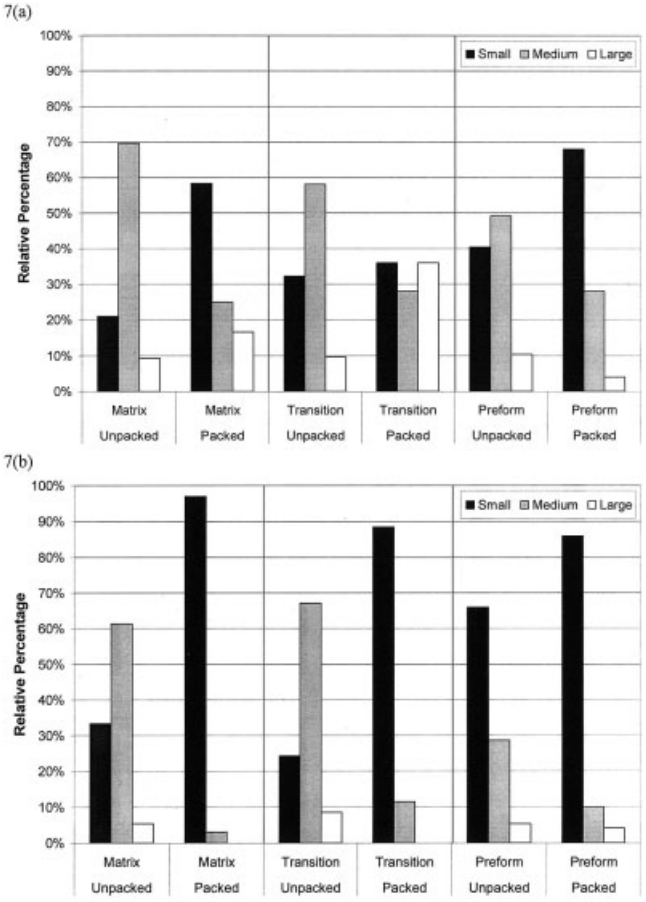

FIG. 7. (a) Planar and (b) through-the-thickness size distributions of voids observed in different locations in the unpacked and packed composite disks.

length of 250 μm to 4 mm. Patel and Lee [20] investigated the effects of fiber architecture on void formation in LCM by monitoring the mold filling from a planar plane using model fluids. Although no quantifications were given, they reported the formation of voids with different shapes for both bidirectional stitched fiberglass and 4-harness woven fiberglass preforms. These different void shapes observed in RTM and LCM composites can originate from different wetting mechanisms for different preform architectures. For instance, a fast flow impregnating unidirectional fiber tows in the transverse direction is expected to trap cylindrical intra-tow voids, while voids trapped around a preform stitch by a slow impregnating flow are reported to be mostly irregular [22–25].

Figure 8 depicts representative images of voids with different shapes encountered in the unpacked composite obtained at 200× magnification from through-the-thickness and planar views. Voids seen in Fig. 3b and top left of Fig. 8d are mostly circular. In contrast, voids trapped between fiber bundles in the bottom of Fig. 8a and top of Fig. 8c are more elliptical. Voids entrapped within the preform in Fig. 3a and bottom of Fig. 8c present a different irregular geometry. Another void shape is large, cigar-shaped, preform voids observed only in the planar view as seen in Fig. 8b,d. These cylindrical voids appear only as smaller truncated voids when observed from a through-the-thickness surface.

First, based on the observed shapes, voids are separated into three groups: irregular, cylindrical, and spherical voids. Irregular voids are defined as those presenting a nonconvex planar surface area, that is, two different points exist within the void that can be connected by a straight line that intersects the void boundary. Cylindrical voids are defined as cigar-shaped voids, found exclusively inside fiber bundles (Fig. 8b,d). Excluding those two categories, the remaining voids are mostly spherical, even though most of them do not present a perfect circular symmetry. To classify this variation in voids' roundness, void data is further processed by introducing the shape ratio, R_s, defined for each void as the equivalent diameter obtained from *Eq. 1* divided by the maximum measured length, L_{max}, within a void:

$$R_s = \frac{D_{eq}}{L_{\max}}. \tag{2}$$

Note that ideal circles are represented by $R_s = 1$, and as the shape ratio gets smaller, voids become more elongated. Using this shape ratio, spherical voids are further segregated into two categories: circular voids with shape ratios above 0.95 ($0.95 < R_s \leq 1$), and elliptical voids with shape ratios lower than 0.95. Different shape parameters are utilized for roundness measurement of voids in composites [8, 28–31], or pores in both ceramics [47, 50] and metals [53].

Using the criteria defined above, contributions to void content from voids with different shapes are calculated. The resulting shape distributions of voids observed in unpacked and packed composites are presented in Fig. 9a,b. Shape distributions based on void areal densities obtained from both planar and through-the-thickness surfaces are simultaneously analyzed in order to assess the accurate void morphology. Circular voids are almost completely removed, with a 99.2% reduction in void areal density when assessed from the planar views. An equally high, 98.0% void removal rate is observed for circular voids when evaluated using the through-the-thickness view. Cylindrical voids can only be seen in the planar view as the through-the-thickness sample is cut perpendicularly to most fiber bundles—potential beds for cylindrical voids. Packing is found to reduce the void areal density of cylindrical voids from 0.86 to 0.14 voids/mm^2, registering an 83.0% reduction rate.

Elliptical and irregular voids both show a slightly different percentage reduction in void areal densities. Contribution of elliptical voids to planar void areal density decreases from 0.9 voids/mm^2 in the unpacked composite to 0.2 voids/mm^2 in the packed composite, while its through-the-thickness counterpart drops from 2.9 to 0.6 voids/mm^2. These reductions of 66.7 and 81.1% are significant voidage removal levels even if they are lower than those observed for circular and cylindrical voids. Likewise, although areal densities of irregular voids assessed from both surfaces drop considerably (i.e., 37.5% in the planar surface and 70.3% in

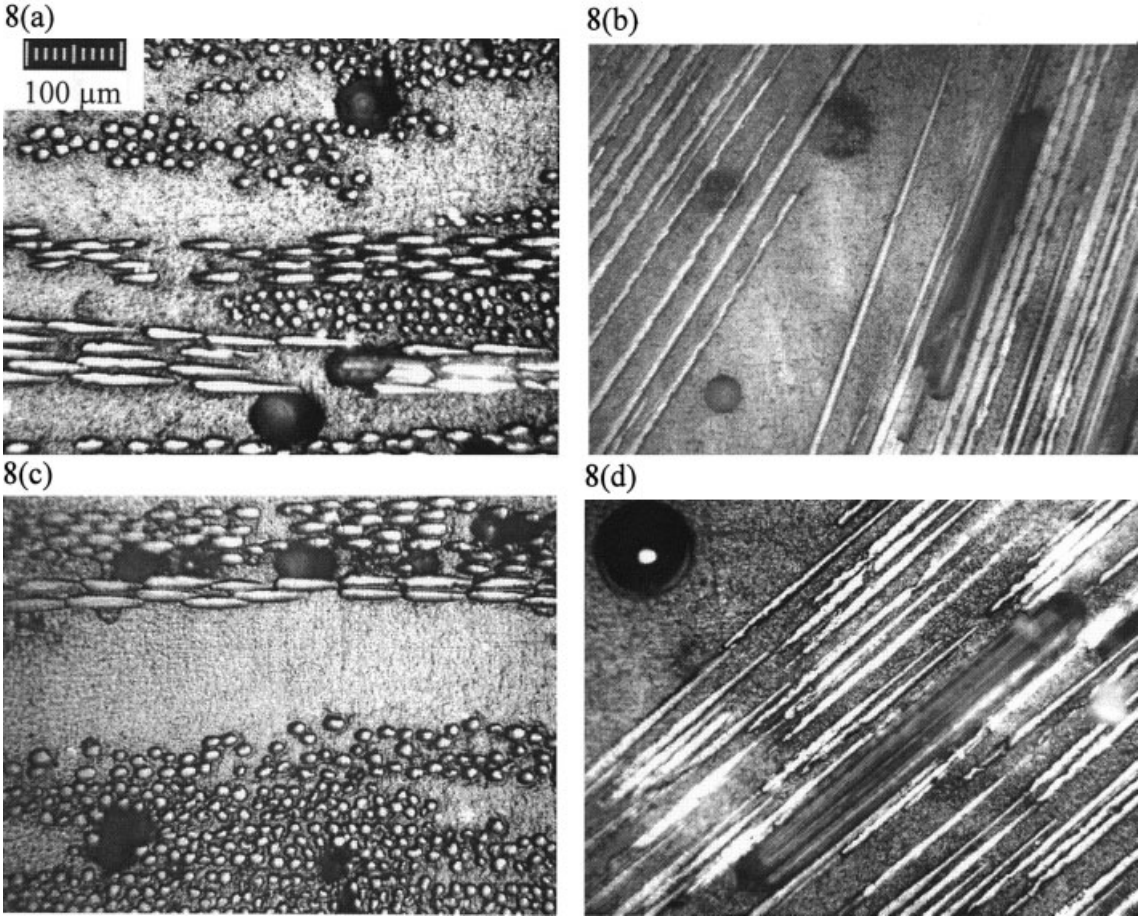

FIG. 8. Representative images of voids with different shapes obtained at 200× magnification from through-the-thickness (left column) and planar (right column) views of the unpacked composite disk.

the through-the-thickness view), these removal rates do not reach the reduction levels of circular and cylindrical voids. These findings show that voids with different shapes do not have the same likelihood of removal under packing. Irregular and elliptical voids are found to be less sensitive to packing than cylindrical and circular voids.

Data of irregular voids obtained from all four samples are further processed to obtain their size distribution. The resulting size distributions of irregular voids in unpacked and packed composites are depicted in Fig. 10. Based on through-the-thickness data, all irregular voids with different sizes are observed to decrease. As a result of packing, irregular small voids dropped from 2.0 to 0.9 voids/mm^2. Medium and large voids experienced even higher removal rates, decreasing respectively from 1.3 and 0.2 voids/mm^2 to 0.1 and 0.03 voids/mm^2, which corresponds to 81.6 and 76.9% reductions. The very low planar areal densities of irregular voids are also depicted in Fig. 10 to ascertain that no increase in large irregular voids occurs in the packed composite. These results show that insignificant occurrences of large irregular voids are present in the packed composite and, in any case, their incidence level is significantly lower than those experienced in the unpacked composite.

The shape ratio defined earlier can help monitor void elongation due to shear induced by packing. An analysis using the shape ratio was undertaken to shed some light on the size distribution of transition voids depicted in Fig. 7. Using planar data of all voids from both unpacked and packed composites, average shape ratios of both total and transition voids were calculated and presented in Table 1, along with their respective 95% confidence intervals and standard deviations. Packing is found to produce on average more elongated voids, as the average shape ratio dropped from 0.84 to 0.67, given that circular voids with the highest shape ratios are almost entirely eliminated, as shown in Fig. 9. Transition voids see a more accentuated elongation due to packing since their average shape ratio is reduced from 0.98 to 0.66, possibly due to shear deformation of the voids restrained by the neighboring fibers.

Effect of Packing on Radial Voidage Variation

Variation of void content in the radial direction in both composites was examined to assess packing effects on spatial void distribution, and ensure that anomalies in void concentration are not formed. Five radial regions of equal length, covering the entire composite samples, are defined

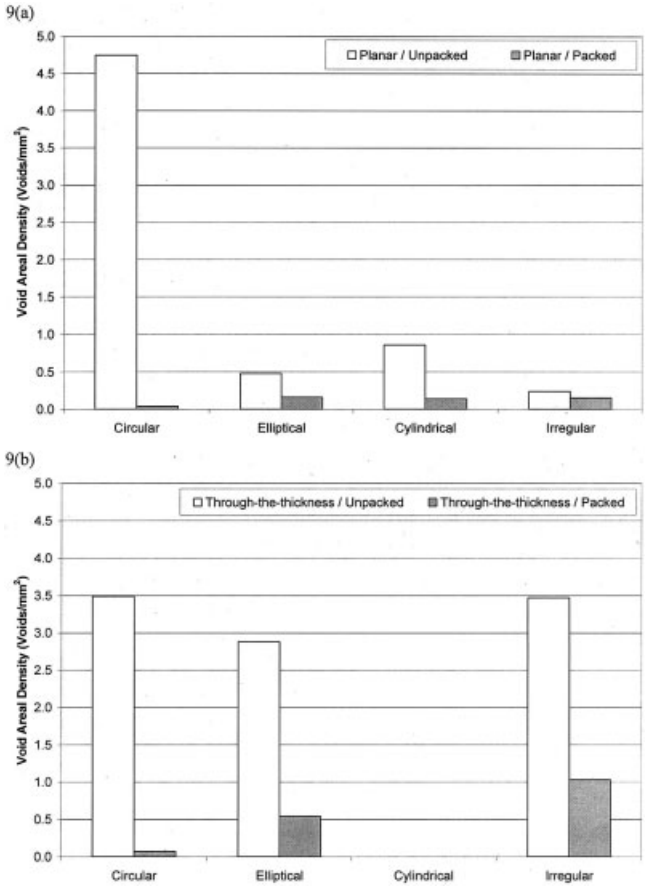

FIG. 9. (a) Planar and (b) through-the-thickness void shape distributions for the unpacked and packed composite disks.

as shown in Fig. 2b,c for both the planar and through-the-thickness surfaces, respectively. Figure 11 illustrates the variation of void content in the radial direction obtained from planar and through-the-thickness surfaces for the unpacked and packed composites. Radial variation of void content of the unpacked composite seems to show a very slight increase in the voidage away from the injection gate. Concurrently, the packed composite depicts different radial trends of void content from both views. From the planar view, void content in the packed composite slightly increases through the first three radial regions from 0.3 to 0.4%, and then drops dramatically in the last two regions. In contrast, from through-the-thickness view, void content in the packed composite, with the exception of the first radial region, is observed to increase almost linearly with radial distance from the injection gate, doubling from 0.1 to 0.2% between the second and fifth region. We submit that the spatial variation of voidage in the packed composite can be attributed to the voids' existing predispositions to removal before packing, influenced by their proximity to fibers. Note that proximity to fibers was classified based on the location of voids earlier in this article. Still, voidage levels are very low in all radial regions of the packed composite and voids do not seem to concentrate radially at any particular region and a structurally weak radial position is not expected.

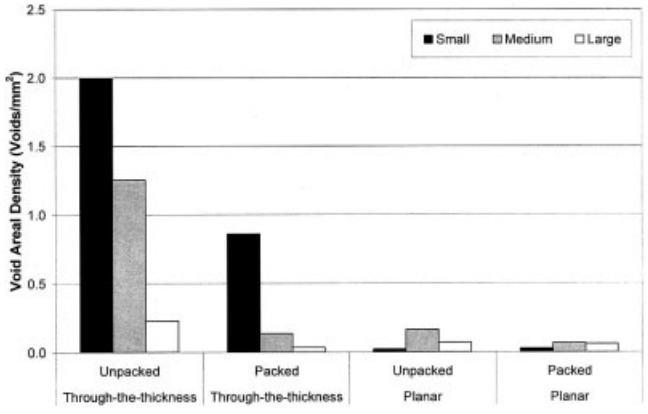

FIG. 10. Through-the-thickness and planar size distributions of irregular voids obtained from the unpacked and packed composite disks.

To further investigate the radial variation of void content in the packed composite, contribution of voids from different locations to the overall void content is considered. As discussed above, through-the-thickness surface is likely to better represent the distribution of void locations. Thus, only through-the-thickness void data are utilized in the following analysis. The effect of location of voids on reduction rates in each radial region can be studied by introducing a *conformity parameter*, $C_{i,l}$, defined as:

$$C_{i,l} = \frac{R_{i,l} - R_i}{R_i}, \tag{3}$$

where R_i is the reduction rate for all voids at the radial region i, and $R_{i,l}$ the reduction rate for voids formed at a particular location l. Note that there are five regions, $i = 1$–5, and three void locations, l = matrix, transition, or preform. A positive conformity parameter means that voids at that particular location have experienced a higher reduction rate than the reduction rate experienced by all voids combined in that radial region, and vice versa.

Figure 12 depicts radial variations of conformity parameter for matrix, transition, and preform voids obtained from the through-the-thickness surface. The first observation is that void content reduction rates of voids formed in different locations, depicted in Fig. 5b, are not uniform at a particular region or along the radius of the composite. Voids in different locations of the composite respond differently to packing. For instance, in the second radial region, transition voids are more prone to removal by packing than matrix and preform voids. In addition to voids' proximity to fibers, their radial position seems to affect the reduction rates. Unlike the first region, matrix voids have a much higher reduction rate than transition and preform voids in the fourth and fifth regions.

Conformity parameter of matrix voids shows a steady increase from –18.1% in the first radial region to a high of 11.6% in the fifth. Matrix voids experience a considerably lower reduction rate than transition and preform voids in the

TABLE 1. Effect of applying a 570 kPa postfill pressure on shape ratio distribution for the overall composite and for transition voids.

	Overall voids	Transition voids
Unpacked composite	Average shape ratio: 0.8347 ± 0.0097 Standard deviation: 0.1798	Average shape ratio: 0.9778 ± 0.0063 Standard deviation: 0.0487
Packed composite	Average shape ratio: 0.6658 ± 0.0174 Standard deviation: 0.2031	Average shape ratio: 0.6577 ± 0.0724 Standard deviation: 0.1847

first radial region. Along the radial direction, matrix voids gradually see their reduction rate increase reaching a much higher rate than transition and preform voids in the fifth region. This monotonic raise is attributed to preexisting voidage arrangement in the composite disk prior to packing. Data collected from the unpacked composite show that matrix voids become smaller away from the injection gate. Smaller matrix voids, in turn, are easier to dissolve under pressure. Therefore, more matrix voids might be dissolved into the matrix near the exit vents. One should keep in mind, nonetheless, that matrix voids are a very small portion (less than 7%) of all voids existing in the unpacked composite.

Preform voids show negative values of conformity parameter in all radial regions, while transition voids are observed to have solely positive values. As seen in Fig. 5b, preform voids are less prone to removal by packing. Therefore, negative values of preform conformity parameter are expected. Transition voids are also anticipated to be more susceptible to pressure-induced shrinkage or removal than preform voids since they are directly subjected to the higher packing pressure. The highest negative conformity parameter for preform voids, i.e., 15.2%, is observed at 67.5 mm away from the injection gate. Region five has the lowest occurrence of preform voids prior to packing, with mostly small voids. Small preform voids, situated well inside fiber tows, might be more difficult to remove since they are shielded from the packing pressure. In contrast, large preform voids often wrap around a large part of the fiber tow, making them more susceptible to the packing pressure. Incidentally, preform voids show their lowest conformity parameter in the first radial region, which experiences the highest fluid front velocity during injection, and thus has the maximum occurrence of large preform voids. A similar analysis can be conducted on transition voids for all radial regions. In short, the levels of removal of voids with different proximities to fibers, although comparable, are governed by their preexisting arrangement at the end of the filling stage, i.e., prior to packing. This finding further stresses the importance of understanding spatial void morphology in LCM composites in order to implement proper void removal methods.

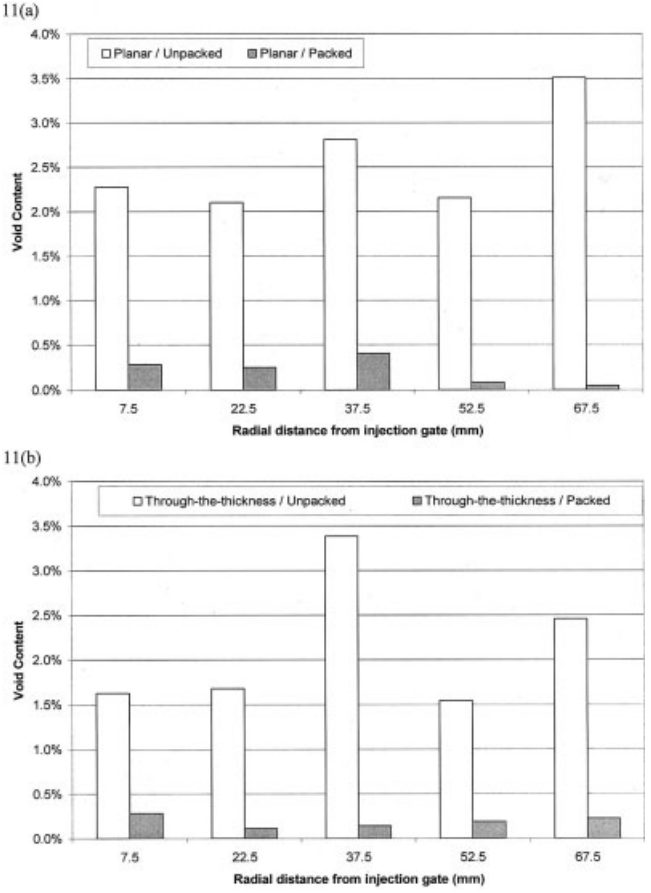

FIG. 11. Radial variation of void content in the unpacked and packed composite disks: (a) obtained from the planar surface, and (b) obtained from the through-the-thickness surface.

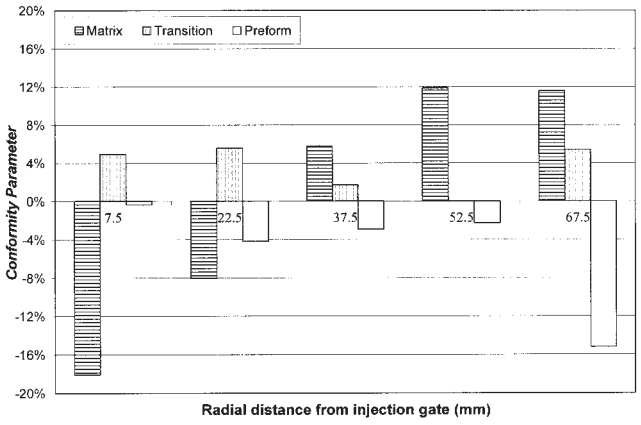

FIG. 12. Through-the-thickness radial variation of conformity parameter from average void content reduction rates due to the application of 570 kPa postfill pressure.

CONCLUSIONS

The effects of applying a postfill pressure on void content, void morphology, and void spatial distribution are presented for RTM E-glass/epoxy composites containing 17.5% fibers. The composite molded with a 570 kPa packing pressure showed an almost 92% drop in void content compared to an unpacked composite. Microscopic image analysis was utilized to examine voidage from both through-the-thickness and planar surfaces of the two molded disks. Only 0.2% void content was registered in the packed composite, whereas the unpacked composite showed void contents of 2.2 and 2.6% in the through-the-thickness and planar surfaces, respectively. In addition, the average void size was observed to decrease from 59.3 μm in the unpacked composite to 31.7 μm in the packed composite when observed from through-the-thickness surface. A comparable reduction rate was observed on the planar surface from 66.7 to 41.1 μm in average void size. Furthermore, reduction rates of voids appear to be affected by their shapes. While circular voids experienced the highest removal rate of 99%, cylindrical and elliptical voids registered lower but still significant reduction rates of 83 and 81%, respectively. Irregular voids, on the other hand, showed a slightly lower void removal rate at 67%. Proximity of voids to fiber bundles was also observed to affect their removal rates, as voids located inside fiber tows sustained slightly lower reduction rates. Along the radial direction, removal of voids with different proximities to fibers seems to depend on their arrangement at the end of the filling stage. These findings are believed to be relevant to RTM and LCM processes with similar flow kinetics. Finally, packing did not induce any spatial void concentration or other adverse effects, thus validating packing as an effective void removal method.

REFERENCES

1. D. Abraham and R. McIlhagger, *Compos. Part A*, **29**, 533 (1998).
2. D. Abraham, S. Matthews, and R. McIlhagger, *Compos. Part A*, **29**, 795 (1998).
3. C.F. Johnson, *Composite Materials Technology—Process and Properties*, Ch. 5, Hanser, New York (1990).
4. C.A. Howe, R.J. Paton, and A.A. Goodwin, *Proc. ICCM-11, Composites Processing and Microstructure*, Australian Composite Structures Society, Gold Coast, Australia, 46 (1997).
5. N.C.W. Judd and W.W. Wright, *SAMPE J.*, **14**, 10 (1978).
6. S. Govindarjan and N.A. Langrana, *F. E. Anal. Design*, **23**, 333 (1996).
7. S.R. Ghiorse, *SAMPE Q.*, Jan., 54 (1993).
8. K.A. Olivero, H.J. Barraza, E.A. O'Rear, and M.C. Altan, *J. Compos. Mater.*, **36**, 2011 (2002).
9. A.A. Goodwin, C.A. Howe, and R.J. Paton, *Proc. ICCM-11, Composites Processing and Microstructure*, Australian Composite Structures Society, Gold Coast, Australia, 11 (1997).
10. N. Pearce, F. Guild, and J. Summerscales, *Compos. Part A*, **29**, 141 (1998).
11. M.R. Wisnom, T. Reynolds, and N. Gwilliam, *Compos. Sci. Tech.*, **56**, 93 (1996).
12. K.J. Bowles and S. Frimpong, *J. Compos. Mater.*, **26**, 1487 (1992).
13. B.D., Harper, G.H. Staab, and R.S. Chen, *J. Compos. Mater.*, **21**, 280 (1987).
14. C. Hoppel, T. Bogettiand, and J.F. Newill, *Proc. Am. Soc. Compos., APG*, MD, 1094 (2000).
15. R. Gebart and L. Strömbeck, *Principles of Liquid Composite Molding*, Carl Hanser, Munich, 358 (2000).
16. S.-B. Shim, J.C. Seferis, and W. Hudson, *J. Adv. Mater.*, **28**, 26 (1997).
17. M.M. Thomas, B. Joseph, and J.L. Kardos, *Polym. Compos.*, **18**, 283 (1997).
18. K. Han and L.J. Lee, *J. Compos. Mater.*, **30**, 1458 (1996).
19. A.D. Mahale, R.K. Prud'Homme, and L. Rebenfeld, *Polym. Eng. Sci.*, **32**, 319 (1992).
20. N. Patel and L.J. Lee, *Polym. Compos.*, **16**, 386 (1995).
21. N. Patel, V. Rohatgi, and L.J. Lee, *Polym. Eng. Sci.*, **35,** 837 (1995).
22. V. Rohatgi, N. Patel, and L.J. Lee, *Polym. Compos.*, **17**, 161 (1996).
23. N. Patel and L.J. Lee, *Polym. Compos.*, **17**, 96 (1996).
24. M.K. Kang, W.I. Lee, and H.T. Hahn, *Compos. Sci. Tech.*, **60**, 2427 (2000).
25. T.S. Lundstrom and B.R. Gebart, *Polym. Compos.*, **15**, 25 (1994).
26. T.S. Lundstrom, B.R. Gebart, and C.Y. Lundemo, *J. Reinf. Plas. Compos.*, **12**, 1339 (1993).
27. H.P.G. Darcy, *Les Fontaines Publiques de la Ville de Dijon,* Delmont, Paris, 306 (1856).
28. K.A. Olivero, Y.K. Hamidi, L. Aktas, and M.C. Altan, *J. Compos. Mater.*, **38**, 937 (2004).
29. H.J. Barraza, Y.K. Hamidi, L. Aktas, E.A. O'Rear, and M.C. Altan, *J. Compos. Mater.*, **38**, 195 (2004).
30. Y.K. Hamidi, L. Aktas, and M.C. Altan, *Compos. Sci. Tech.*, **65**, 1306 (2005).
31. Y.K. Hamidi, L. Aktas, and M.C. Altan, *J. Eng. Mater. Tech.*, **126**, 420 (2004).
32. A.W. Chan and R.J. Morgan, *SAMPE Q.*, April, 48 (1992).
33. N. Patel and L.J. Lee, *Polym. Compos.*, **17**, 104 (1996).
34. C. Binetruy, B. Hilaire, and J. Pabiot, *J. Compos. Mater.*, **32**, 223 (1998).
35. K. Han and L.J. Lee. *J. Compos. Mater.*, **30**, 1458 (1996).
36. C.-Y. Chang and L.-W. Hourng, *Polym. Eng. Sci.*, **38**, 809 (1998).
37. J. Breard, A. Saouab, and G. Bouquet, *Compos. Part A*, **34**, 517 (2003).
38. A. Shojaei, S.R. Ghaffarian, and S.M.H. Karimian, *Polym. Compos.*, **24**, 525 (2003).
39. W.R. Stabler, G.B. Tatterson, R.L. Sadler, and A.H.M. El-Shiekh, *SAMPE Q.*. Jan., 38 (1992).
40. W.K. Chui, J. Glimm, F.M. Tangerman, A.P. Jardine, J.S.

Madsen, T.M. Donnellan, and R. Leek, *Proc. 9th Int. Conf. Numer. Methods Thermal Problems*, Atlanta, 1323 (1995).

41. N. Ikegawa, H. Hamada, and Z. Maekawa, *Polym. Eng. Sci.*, **36**, 953 (1996).
42. J.H. Choi and C.K.H. Dharan, *J. Compos. Mater.*, **36**, 2267 (2002).
43. S.R. Ghiorse, *U.S. Army Mater. Tech. Lab. Report MTL TR*, 91 (1991).
44. C. Santulli, R. Garcia Gil, A.C. Long, and M.J. Clifford, *Sci. Eng. Compos. Mater.*, **10**, 77 (2002).
45. H. Jiang, P. Bowen, and J.F. Knott, *J. Mater. Sci.*, **34**, 719 (1999).
46. M. Singh, M.K. Trivedi, and J. Bellare, *J. Mater. Sci.*, **34**, 5315 (1999).
47. C. Kawai, *J. Mater. Sci.*, **36**, 5713 (2002).
48. R. Chaim and M. Hafetz. *J. Mater. Sci.*, **39**, 3057 (2004).
49. R.W. Rice, *J. Mater. Sci.*, **34**, 2769 (1999).
50. T. Fukasawa, Z.-Y. Deng, M. Ando, T. Ohji, and Y. Goto, *J. Mater. Sci.*, **36**, 2523 (2001).
51. Y. Sun, G. Liu, and C. Wang, *J. Mater. Sci.*, **39**, 2553 (2004).
52. X. Song and G. Liu, *J. Mater. Sci.*, **34**, 2433 (1999).
53. B. Kubicki, V. Sundhar, and M. Kubicki, *J. Mater. Sci.*, **37**, 3959 (2002).